Pergamon

Int. J. Heat Mass Transfer. Vol. 38, No. 14, pp. 2647–2655, 1995

0017-9310/95 $9.50+0.00

0017-9310(94)00347-5

Momentum transfer at the boundary between a porous medium and a homogeneous fluid—II. Comparison with experiment

J. ALBERTO OCHOA-TAPIA
Departamento de Ingeniería Química, Instituto Tecnológico de Celaya 38010 Celaya, Gto. México

and

STEPHEN WHITAKER†
Department of Chemical Engineering, University of California at Davis, Davis, CA 95616, U.S.A.

(*Received* 20 *May* 1994 *and in final form* 4 *November* 1994)

Abstract—In Part I of this paper a stress jump condition was developed based on the non-local form of the volume averaged Stokes' equations. The excess stress terms that appeared in the jump condition were represented in a manner that led to a tangential stress boundary condition containing a single adjustable coefficient of order one. In this paper we compare the theory with the experimental studies of Beavers and Joseph [*J. Fluid Mech.* **30**, 197–207 (1967)], and we explore the use of a variable porosity model as a substitute for the jump condition. The latter approach does not lead to a successful representation of all the experimental data, but it does provide some insight into the complexities of the boundary region between a porous medium and a homogeneous fluid.

1. INTRODUCTION

The analysis presented in Part 1 of this paper dealt with the general problem of momentum transfer at the boundary between a porous medium and a homogeneous fluid. We have illustrated such a boundary in Fig. 1 where the porous medium is represented by the ω-region and the homogeneous fluid by the η-region. When inertial effects are negligible the governing differential equations and boundary conditions can be expressed as

$$\nabla \cdot \langle \mathbf{v}_\beta \rangle_\eta = 0 \quad \text{in the } \eta\text{-region} \tag{1}$$

$$0 = -\nabla \langle p_\beta \rangle_\eta^\beta + \rho_\beta \mathbf{g} + \mu_\beta \nabla^2 \langle \mathbf{v}_\beta \rangle_\eta \quad \text{in the } \eta\text{-region} \tag{2}$$

$$\text{B.C. 1} \quad \langle \mathbf{v}_\beta \rangle_\omega = \langle \mathbf{v}_\beta \rangle_\eta \quad \text{at the } \omega\text{–}\eta \text{ boundary} \tag{3}$$

$$\text{B.C. 2.} \quad \mathbf{n}_{\omega\eta} \cdot [-\mathbf{I}(\langle p_\beta \rangle_\omega^\beta - \langle p_\beta \rangle_\eta^\beta) + \mu_\beta(\varepsilon_{\beta\omega}^{-1} \nabla \langle \mathbf{v}_\beta \rangle_\omega - \nabla \langle \mathbf{v}_\beta \rangle_\eta)]$$
$$= -\mu_\beta \delta \mathbf{D} \cdot [\mathbf{K}_{\beta\omega}^{-1} \cdot \langle \mathbf{v}_\beta \rangle_\omega] + \mu_\beta \delta^{-1} \mathbf{A} \cdot (\varepsilon_{\beta\omega} - 1)^2 (\varepsilon_{\beta\omega}^{-3} \langle \mathbf{v}_\beta \rangle_\omega + \langle \mathbf{v}_\beta \rangle_\eta)$$
$$\text{at the } \omega\text{–}\eta \text{ boundary} \tag{4}$$

$$0 = -\nabla \langle p_\beta \rangle_\omega^\beta + \rho_\beta \mathbf{g} + \varepsilon_{\beta\omega}^{-1} \mu_\beta \nabla^2 \langle \mathbf{v}_\beta \rangle_\omega - \mu_\beta \mathbf{K}_{\beta\omega}^{-1} \cdot \langle \mathbf{v}_\beta \rangle_\omega \quad \text{in the } \omega\text{-region} \tag{5}$$

$$\nabla \cdot \langle \mathbf{v}_\beta \rangle_\omega = 0 \quad \text{in the } \omega\text{-region.} \tag{6}$$

In our analysis of the stress jump condition, we encountered an excess *surface stress*, an excess *bulk stress* and an excess *Brinkman stress*. The excess surface stress does not appear explicitly in equation (4) because it has the same form as the term on the left hand side, while the excess bulk stress and the excess Brinkman stress are represented by the first and second terms respectively on the right hand side. On

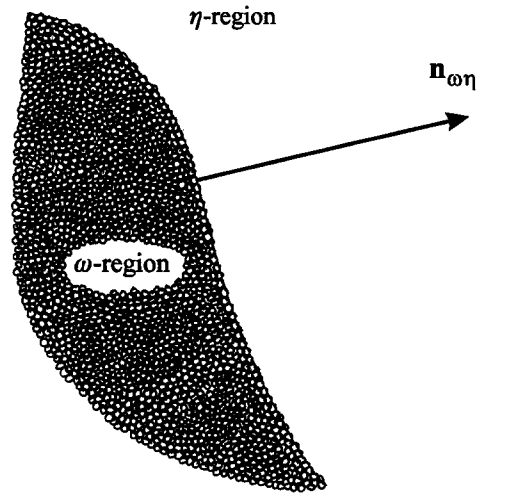

Fig. 1. Boundary between a porous medium and a homogeneous fluid.

†Author to whom correspondence should be addressed.

NOMENCLATURE

D diameter of the averaging volume having the form of a disk [m]
$\mathbf{g}$ gravity vector [m s^{-2}]
h depth of fluid channel [m]
H depth of porous medium [m]
$\mathbf{I}$ unit tensor
$\mathbf{i},\mathbf{j}$ unit base vectors in the x- and y-direction, respectively
$\mathbf{K}_\beta$ Darcy's law permeability tensor [m^2]
K_β norm of the Darcy's law permeability tensor in the interfacial region [m^2]
$\mathbf{K}_{\beta\omega}$ Darcy's law permeability tensor in the homogeneous ω-region [m^2]
$K_{\beta\omega}$ norm of the Darcy's law permeability tensor in the ω-region [m^2]
ℓ_β characteristic length associated with the β-phase in the ω-region [m]
$\mathbf{n}_{\omega\eta}$ unit normal vector directed from the ω-region toward the η-region
$\langle p_\beta\rangle^\beta$ intrinsic average pressure [N m^{-2}]
$\langle p_\beta\rangle^\beta_\omega$ intrinsic average pressure in the ω-region [N m^{-2}]
$\langle p_\beta\rangle^\beta_\eta$ intrinsic average pressure in the η-region [N m^{-2}]
$\langle \mathbf{v}_\beta\rangle$ superficial average velocity [m s^{-1}]
$\langle \mathbf{v}_\beta\rangle_\omega$ superficial average velocity in the ω-region [m s^{-1}]
$\langle \mathbf{v}_\beta\rangle_\eta$ superficial average velocity in the η-region [m s^{-1}]
x, y rectangular coordinates [m].

Greek symbols

α the adjustable coefficient in the Beavers and Joseph jump condition
β the adjustable coefficient in the representation for the excess stress
Δ thickness of a disk that represents an averaging volume [m]
δ thickness of the interfacial region [m]
ε_β porosity or volume fraction of the β-phase
$\varepsilon_{\beta\omega}$ porosity in the homogeneous portion of the ω-region
μ_β viscosity of the β-phase [N s m^{-2}]
ρ_β density of the β-phase [kg m^{-3}].

Subscripts

β identifies a quantity associated with the β-phase
η identifies a quantity associated with the η-region
ω identifies a quantity associated with the ω-region
$\omega\eta$ identifies a quantity associated with the ω–η boundary.

Superscripts

β identifies an intrinsic volume average.

the basis of equation (3) we can express the stress jump condition in the compact notation represented by

B.C. 3′

$$\mathbf{n}_{\omega\eta}\cdot[-\mathbf{I}(\langle p_\beta\rangle^\beta_\omega-\langle p_\beta\rangle^\beta_\eta)+\mu_\beta(\varepsilon^{-1}_{\beta\omega}\nabla\langle\mathbf{v}_\beta\rangle_\omega-\nabla\langle\mathbf{v}_\beta\rangle_\eta)] = \mu_\beta\mathbf{M}\cdot\langle\mathbf{v}_\beta\rangle_\omega \quad \text{at the } \omega\text{–}\eta \text{ boundary.} \tag{7}$$

If the thickness of the boundary region can be scaled according to $\delta = \mathbf{O}\sqrt{(K_{\beta\omega})}$, we see from equations (4) and (7) that the tensor $\mathbf{M}$ will depend on both $K_{\beta\omega}$ and $\varepsilon_{\beta\omega}$. For the one-dimensional flow process illustrated in Fig. 2, we require only the x-component of equations (1)–(7), along with the boundary conditions at $y = h$ and $y = -H$. If the Brinkman correction is negligible at $y = -H$, the boundary value problem describing the flow illustrated in Fig. 2 can be expressed as

B.C 1 $\langle v_\beta\rangle_\eta = 0, \quad y = h$ no slip condition (8)

$$0 = -\frac{\partial\langle p_\beta\rangle^\beta_\eta}{\partial x}+\mu_\beta\frac{\partial^2\langle v_\beta\rangle_\eta}{\partial y^2} \qquad 0 \leqslant y \leqslant h \quad \text{Stokes' equations} \tag{9}$$

B.C. 2

$$\langle v_\beta\rangle_\eta = \langle v_\beta\rangle_\omega \quad y = 0 \quad \text{continuity of velocity} \tag{10}$$

B.C. 3

$$\frac{1}{\varepsilon_{\beta\omega}}\frac{\partial\langle v_\beta\rangle_\omega}{\partial y}-\frac{\partial\langle v_\beta\rangle_\eta}{\partial y}=\frac{\beta}{\sqrt{(K_{\beta\omega})}}\langle v_\beta\rangle_\omega, \quad y = 0$$

stress jump condition (11)

$$0 = -\frac{\partial\langle p_\beta\rangle^\beta_\omega}{\partial x}+\frac{\mu_\beta}{\varepsilon_{\beta\omega}}\frac{\partial^2\langle v_\beta\rangle_\omega}{\partial y^2}-\frac{\mu_\beta}{K_{\beta\omega}}\langle v_\beta\rangle_\omega, \quad -\infty < y < 0$$

Darcy's law with the first Brinkman correction (12)

B.C. 4 $\langle v_\beta\rangle_\omega$ is bounded as $y \to -\infty$. (13)

Here we have used $\langle v_\beta\rangle_\omega$ and $\langle v_\beta\rangle_\eta$ to represent the x-components of the two volume average velocity vectors, and the dimensionless coefficient β is given by

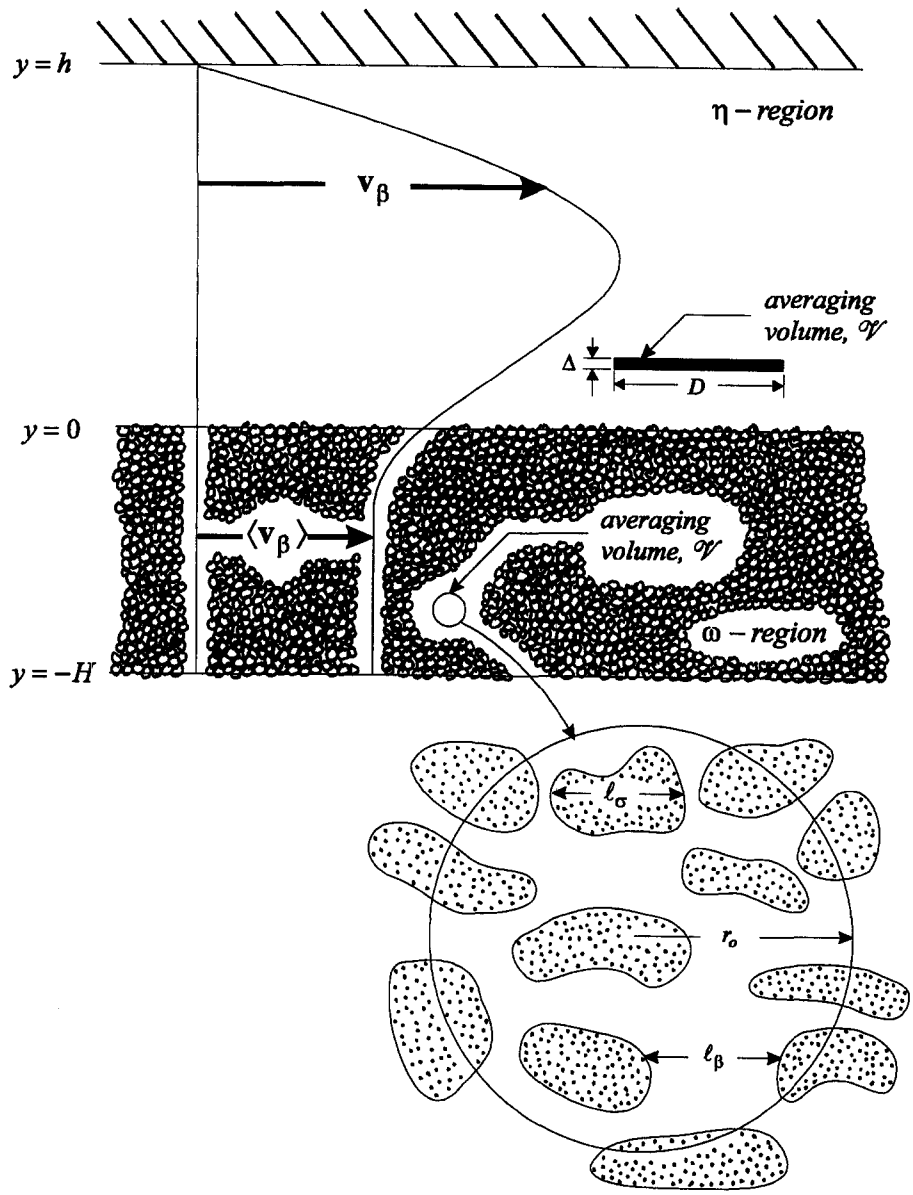

Fig. 2. Flow of a homogeneous fluid parallel to a porous medium.

$$\beta = \sqrt{(K_{\beta\omega})}[\delta^{-1}\mathbf{i}\cdot\mathbf{A}\cdot\mathbf{i}(\varepsilon_{\beta\omega}-1)^2(\varepsilon_{\beta\omega}^{-3}+1) - \delta\mathbf{i}\cdot\mathbf{D}\cdot\mathbf{K}_{\beta\omega}^{-1}\cdot\mathbf{i}]. \quad (14)$$

We expect the dimensionless coefficient β to be on the order of one, and because of the nature of excess functions we can expect that β may be either positive or negative. It is of some importance to note that the coefficient β depends on the parameter $\sqrt{(K_{\beta\omega})}/\delta$ and on the inverse of this parameter, $\delta/\sqrt{(K_{\beta\omega})}$, and we express this idea as

$$\beta = \mathbf{O}\left(\frac{\sqrt{(K_{\beta\omega})}}{\delta}, \frac{\delta}{\sqrt{(K_{\beta\omega})}}\right). \quad (15)$$

In the next section we will compare solutions of equations (8)–(13) with the experimental data of Beavers and Joseph [1].

2. COMPARISON WITH EXPERIMENT

In solving equations (8)–(13) we can make use of the fact that the pressure gradients are constant and equal to each other

$$\frac{\partial\langle p_\beta\rangle_\omega^\beta}{\partial x} = \frac{\partial\langle p_\beta\rangle_\eta^\beta}{\partial x} = \text{constant} \quad (16)$$

so that the dimensionless form of our boundary value problem is given by

B.C. 1 $$U_\eta = 0 \quad \text{at } Y = \sigma \quad (17)$$

$$\frac{d^2U_\eta}{dY^2} = -1, \quad 0 \leqslant Y \leqslant \sigma \quad (18)$$

B.C. 2 $$U_\eta = U_\omega, \quad Y = 0 \quad (19)$$

B.C. 3 $$\frac{1}{\varepsilon_{\beta\omega}}\frac{dU_\omega}{dY}-\frac{dU_\eta}{dY}=\beta U_\omega \quad \text{at } Y=0 \tag{20}$$

$$\frac{1}{\varepsilon_{\beta\omega}}\frac{d^2U_\omega}{dY^2}-U_\omega=-1, \quad -\infty \leqslant Y \leqslant 0 \tag{21}$$

B.C. 4 $$U_\omega \to 1 \quad \text{at } Y \to -\infty. \tag{22}$$

Here we have made use of the following dimensionless variables

$$Y=\frac{y}{\sqrt{(K_{\beta\omega})}} \tag{23}$$

$$U_\omega=\frac{\langle v_\beta\rangle_\omega}{\langle v_\beta\rangle_\omega^\infty} \tag{24}$$

$$U_\eta=\frac{\langle v_\beta\rangle_\eta}{\langle v_\beta\rangle_\omega^\infty}. \tag{25}$$

In terms of these variables, and the three parameters σ, β and $\varepsilon_{\beta\omega}$, the solutions for the two velocities can be expressed as

$$U_\eta=\tfrac{1}{2}\sigma^2[1-(Y/\sigma)^2]-C_1\sigma[1-(Y/\sigma)], \quad 0 \leqslant Y \leqslant \sigma \tag{26}$$

$$U_\omega=C_2\exp(\sqrt{(\varepsilon_{\beta\omega})}\,Y)+1, \quad -\infty \leqslant Y \leqslant 0. \tag{27}$$

Here we have followed the nomenclature of Beavers and Joseph [1] and used σ to represent the dimensionless channel depth.

$$\sigma=h/\sqrt{(K_{\beta\omega})}. \tag{28}$$

The two constants of integration in the expressions for the velocity are given by

$$C_1=\frac{\tfrac{1}{2}\sigma^2(1-\beta\sqrt{(\varepsilon_{\beta\omega})})-1}{(1-\beta\sigma)\sqrt{(\varepsilon_{\beta\omega})}+\sigma} \tag{29}$$

$$C_2=\frac{(C_1+\beta)\sqrt{(\varepsilon_{\beta\omega})}}{1-\beta\sqrt{(\varepsilon_{\beta\omega})}}. \tag{30}$$

When β is set equal to zero, equations (26)–(30) reduce to the Brinkman model.

2.1. *Comparison with experimental data*

The original comparison between theory and experiment was carried out by Beavers and Joseph [1] in terms of the flow rate in the channel illustrated in Fig. 2 relative to the flow rate that would occur if the porous media were impermeable. The ratio of flow rates can be expressed in terms of the ratio of area averaged velocities, and in the η-region the area averaged, dimensionless velocity is given by

$$\langle U_\eta\rangle=\frac{1}{\sigma}\int_{Y=0}^{Y=\sigma}U_\eta\,dY=\tfrac{1}{3}\sigma^2-\tfrac{1}{2}\sigma C_1. \tag{31}$$

For the case in which the permeability tends to zero, $K_{\beta\omega}\to 0$, we designate the dimensionless average velocity in the η-region by $\langle U_\eta\rangle^*$ and note that equation (31) leads to

$$\langle U_\eta\rangle^*=\tfrac{1}{12}\sigma^2. \tag{32}$$

Following Beavers and Joseph [1], the fractional increase in the flow is expressed as

$$\Phi=\frac{\langle U_\eta\rangle}{\langle U_\eta\rangle^*}-1 \tag{33}$$

and when equations (29), (31) and (32) are used we obtain

$$\Phi=\frac{3(\sigma+2/\sqrt{(\varepsilon_{\beta\omega})})}{\sigma(1-\beta\sigma+\sigma/\sqrt{(\varepsilon_{\beta\omega})})}. \tag{34}$$

When β is equal to zero we recover the Brinkman solution which leads to a fractional excess flow given by

$$\Phi=\frac{3(\sigma+2/\sqrt{(\varepsilon_{\beta\omega})})}{\sigma(1+\sigma/\sqrt{(\varepsilon_{\beta\omega})})} \quad \text{Brinkman solution.} \tag{35}$$

This result has exactly the same *form* as that of Beavers and Joseph [1]; however, in this case there is no adjustable parameter. To be clear about this matter, we list the result of Beavers and Joseph as

$$\Phi=\frac{3(\sigma+2\alpha)}{\sigma(1+\alpha\sigma)} \quad \text{Beavers and Joseph.} \tag{36}$$

Here the dimensionless parameter α results from the stress condition used by Beavers and Joseph which we write in terms of our nomenclature

$$\frac{\partial\langle v_\beta\rangle_\eta}{\partial y}=\frac{\alpha}{\sqrt{(K_{\beta\omega})}}(\langle v_\beta\rangle_\eta-\langle v_\beta\rangle_\omega), \quad y=0 \tag{37}$$

in order to facilitate the comparison with equation (11).

In Figs. 3–5 we compare equation (34) with the experimental data of Beavers and Joseph [1] for various values of the dimensionless, adjustable parameter, β, and we list the Brinkman solution given by equation (35). Since Beavers and Joseph did not measure the porosity of the ω-region, we arbitrarily specified the porosity to be $\varepsilon_{\beta\omega}=0.4$ in both equations (34) and (35). In these figures we see that good agreement between theory and experiment can be obtained for values of β ranging from -1.0 to 1.5. This is consistent

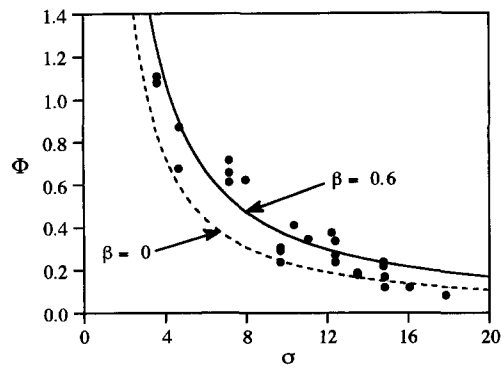

Fig. 3. Comparison between theory and experiment for Foametal ($K_{\beta\omega}=1.1\times10^{-5}$ in^2).

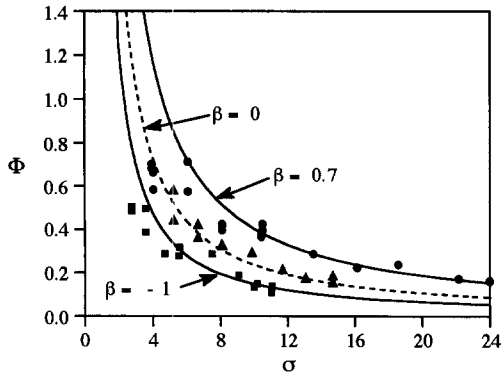

Fig. 4. Comparison between theory and experiment for Foametal (■, $K_{\beta\omega} = 15.0 \times 10^{-6}$ in^2; ▲, $K_{\beta\omega} = 61.0 \times 10^{-6}$ in^2; ●, $K_{\beta\omega} = 127 \times 10^{-6}$ in^2).

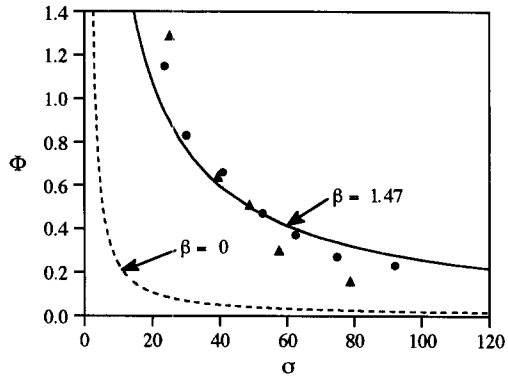

Fig. 5. Comparison between theory and experiment for Aloxite (●, $K_{\beta\omega} = 1.0 \times 10^{-6}$ in^2; ▲, $K_{\beta\omega} = 2.48 \times 10^{-6}$ in^2).

with the idea that β is on the order of one and that the sign of β may be either positive or negative as suggested by the nature of excess functions indicated in Fig. 5 in Part 1. The comparison presented in Fig. 3–5 is analogous to that presented by Beavers and Joseph [1] in their Figs. 4, 6 and 7 where they used equation (36) to obtain similar agreement between theory and experiment. The advantage of our approach is simply that it is a more precise representation of the physics. This is indicated by the fact that β is *order one* whereas the parameter α in equation (36) was varied by a factor of 40 in order to obtain good agreement between equation (36) and the experimental data. The precise comparison between the two approaches is illustrated in Table 1 which is based on Table 1 of Beavers and Joseph [1]. Here one can see that the parameter α is very sensitive to the value of the permeability, $K_{\beta\omega}$, whereas the parameter β is order one for permeabilities that change by a factor of more than 100. It seems clear that this improvement results from the retention of the Brinkman correction term in equation (5). It is also clear that the structure of the porous media, and in particular the structure of the boundary, cannot be described by the single length-scale, $\sqrt{(K_{\beta\omega})}$. If this were the case, a single value of β would suffice to describe the experimental results, whereas the actual values range from -1.0 to $+1.47$.

3. VARIABLE POROSITY MODEL FOR THE BOUNDARY REGION

At this point we return to the general form of the volume averaged Stokes' equations (presented in Section 3 of Part I) which can be expressed as

$$0 = -\nabla\langle p_\beta\rangle^\beta + \rho_\beta \mathbf{g} + \varepsilon_\beta^{-1}\mu_\beta\nabla^2\langle \mathbf{v}_\beta\rangle - \mu_\beta\varepsilon_\beta^{-1}(\nabla\varepsilon_\beta)\cdot[\nabla(\varepsilon_\beta^{-1}\langle \mathbf{v}_\beta\rangle)] - \mu_\beta\boldsymbol{\Phi}_\beta. \quad (38)$$

About the vector $\boldsymbol{\Phi}_\beta$ we know

$$\boldsymbol{\Phi}_\beta = \begin{cases} \mathbf{K}_{\beta\omega}^{-1}\cdot\langle \mathbf{v}_\beta\rangle_\omega & \text{in the homogeneous } \omega\text{-region} \\ 0 & \text{in the homogeneous } \eta\text{-region} \end{cases} \quad (39)$$

and this suggests that we could describe the momentum equation in the boundary region by

$$0 = -\frac{\partial\langle p_\beta\rangle^\beta}{\partial x} + \frac{1}{\varepsilon_\beta(y)}\mu_\beta\frac{\partial^2\langle v_\beta\rangle}{\partial y^2} + \frac{\mu_\beta}{\varepsilon_\beta(y)}\frac{\partial\varepsilon_\beta}{\partial y}\left[\frac{\partial}{\partial y}\left(\frac{1}{\varepsilon_\beta(y)}\langle v_\beta\rangle\right)\right] - \frac{\mu_\beta}{K_\beta(y)}\langle v_\beta\rangle, \quad -\delta \leqslant y \leqslant 0. \quad (40)$$

Here we have explicitly located the boundary region by $-\delta \leqslant y \leqslant 0$ with the thought that this is appropriate for the planar averaging volume shown in Fig.

Table 1. Experimental and theoretical parameters

Block	$K_{\beta\omega}$ [in^2]	α (B and J)	β (This work)	Average pore size [in]
Foametal†	11×10^{-6}	1.2	+0.6	
Foametal A	15×10^{-6}	0.78	+0.7	0.016
Foametal B	61×10^{-6}	1.45	0.0	0.034
Foametal C	127×10^{-6}	4.0	−1.0	0.045
Aloxite	1.0×10^{-6}	0.1	+1.47	0.013
Aloxite	2.48×10^{-6}	0.1	+1.47	0.027

†These results were obtained with water, as opposed to oil, and no estimate of the average pore size was given.

2. If the spherical averaging volume were more appropriate, as it would be if magnetic resonance imaging were used to measure the volume averaged velocity, it would be best to locate the boundary region according to $-\delta/2 \leqslant y \leqslant +\delta/2$. The numerical solution of equation (40) can be coupled with the analytical solutions of equations (9) and (12) in order to produce the velocity field in both the η- and ω-regions, and from those results we can obtain the fractional excess flow denoted by Φ in equation (33).

In the variable porosity model there will be two 'adjustments' that can be made within certain limits. There is the choice of the functional dependence of the porosity in the boundary region, and one must decide on the thickness of the boundary region, δ. The most reliable source of information concerning the latter is the detailed numerical work of Larson and Higdon [2, 3] and of Sahraoui and Kaviany [4]. Their results suggest that the thickness of the boundary region is on the order of the pore or particle diameter associated with the porous media, and to see how this is related to the permeability that has been used as a length-scale parameter for the ω-region, we use the Blake–Kozeny equation [5] to express the permeability as

$$K_{\beta\omega} = \frac{1}{180}\frac{d_p^2 \varepsilon_{\beta\omega}^3}{(1-\varepsilon_{\beta\omega})^2}. \tag{41}$$

In terms of the thickness of the interfacial region, δ, we have

$$\frac{\delta}{\sqrt{(K_{\beta\omega})}} = \left\{\sqrt{\frac{180(1-\varepsilon_{\beta\omega})^2}{\varepsilon_{\beta\omega}^3}}\right\}\left(\frac{\delta}{d_p}\right). \tag{42}$$

For a porosity of $\varepsilon_{\beta\omega} = 0.4$ this leads to the estimate

$$\frac{\delta}{\sqrt{(K_{\beta\omega})}} \approx 30\frac{\delta}{d_p} \tag{43}$$

and on the basis of the work of Larson and Higdon [2, 3] and of Sahraoui and Kaviany [4] we express this idea as

$$\frac{\delta}{\sqrt{(K_{\beta\omega})}} = \mathbf{O}(30). \tag{44}$$

This ratio is related to the parameter α by

$$\frac{1}{\alpha} \approx \frac{\delta}{\sqrt{(K_{\beta\omega})}} \quad \text{or} \quad \alpha = \mathbf{O}(3\times 10^{-2}). \tag{45}$$

Equations (43)–(45) *are consistent* with the results for Aloxite presented in Table 1, but *are not consistent* with the results for Foametal. This is to say that the experimental results of Beavers and Joseph [1] for Foametal are not consistent with the numerical studies of Larson and Higdon [2.3] and of Sahraoui and Kaviany [4] and the idea that δ is on the order of $\sqrt{(K_{\beta\omega})}$.

To be explicit about the solution of the velocity field for the variable porosity model we list the boundary value problem as

B.C. 1 $\langle v_\beta\rangle_\eta = 0, \quad y = h$ no slip condition (46)

$$0 = -\frac{\partial\langle p_\beta\rangle_\eta^\beta}{\partial x} + \mu_\beta\frac{\partial^2\langle v_\beta\rangle_\eta}{\partial y^2},$$

$$0 \leqslant y \leqslant h \quad \text{Stokes' equations} \tag{47}$$

B.C. 2 $\langle v_\beta\rangle_\eta = \langle v_\beta\rangle, \quad \dfrac{\partial\langle v_\beta\rangle_\eta}{\partial y} = \dfrac{\partial\langle v_\beta\rangle}{\partial y},$

$$y = 0 \quad \text{continuity} \tag{48}$$

$$0 = -\frac{\partial\langle p_\beta\rangle^\beta}{\partial y} + \frac{\mu_\beta}{\varepsilon_\beta(y)}\frac{\partial^2\langle v_\beta\rangle}{\partial y^2} + \frac{\mu_\beta}{\varepsilon_\beta(y)}\frac{\partial\varepsilon_\beta}{\partial y}\left[\frac{\partial}{\partial y}\left(\frac{1}{\varepsilon_\beta(y)}\langle v_\beta\rangle\right)\right] - \frac{\mu_\beta}{K_\beta(y)}\langle v_\beta\rangle, \quad -\delta \leqslant y \leqslant 0 \tag{49}$$

variable porosity model

B.C. 3 $\langle v_\beta\rangle = \langle v_\beta\rangle_\omega, \quad \dfrac{\partial\langle v_\beta\rangle}{\partial y} = \dfrac{\partial\langle v_\beta\rangle_\omega}{\partial y},$

$$y = -\delta \quad \text{continuity} \tag{50}$$

$$0 = -\frac{\partial\langle p_\beta\rangle_\omega^\beta}{\partial x} + \frac{\mu_\beta}{\varepsilon_{\beta\omega}}\frac{\partial^2\langle v_\beta\rangle_\omega}{\partial y^2} - \frac{\mu_\beta}{K_{\beta\omega}}\langle v_\beta\rangle_\omega, \quad -\infty < y < -\delta \tag{51}$$

Darcy's law with the first Brinkman correction

B.C. 4 $\langle v_\beta\rangle_\omega$ is bounded as $y \to -\infty$. (52)

For this to be a valid representation, we require that the porosity and the permeability, $\varepsilon_\beta(y)$ and $K_\beta(y)$ be continuous functions and that the porosity have a continuous first derivative. To achieve this, the porosity is expressed as

$$\varepsilon_\beta = 1 + 3(\varepsilon_{\beta\omega}-1)(y/\delta)^2 + 2(\varepsilon_{\beta\omega}-1)(y/\delta)^3, \quad -\delta \leqslant y \leqslant 0 \tag{53}$$

and the functional dependence of the permeability is represented by the Blake–Kozeny equation.

$$\frac{K_{\beta\omega}}{K_\beta(y)} = \frac{(1-\varepsilon_\beta)^2\varepsilon_{\beta\omega}^3}{(1-\varepsilon_{\beta\omega})^2\varepsilon_\beta^3}. \tag{54}$$

While this choice for the porosity and the permeability is plausible, one must keep in mind that other choices could be made; however, once we accept equations (53) and (54) we are left with a single adjustable parameter. This is the thickness of the interfacial region, δ, and we will express this parameter in dimensionless form as, $\delta/\sqrt{(K_{\beta\omega})}$.

The numerical solution of the problem described by equations (46)–(52) makes use of analytical solutions for the η- and ω-region equations given by equations (47) and (51), each of which contains a single undetermined constant of integration. If values for these

two constants are assumed, the velocities at $y = 0$ and $y = -\delta$ are specified and equation (49) can be solved numerically. This produces values of the derivatives of the velocity at $y = 0$ and $y = -\delta$ which are not necessarily equal to the values determined by equations (47) and (51). A Newton–Raphson convergence routine is then used to develop solutions of equations (47), (49) and (51) that provide the continuity conditions listed by equations (48) and (50). Tests showed that the computed results were independent of the mesh size when 200 or more points were used in the finite difference calculations.

In order to clearly identify the solution procedure, we represent equations (46)–(52) in the manner illustrated by equations (17)–(22)

B.C. 1 $$U_\eta = 0 \quad \text{at } Y = \sigma \tag{55}$$

$$\frac{d^2 U_\eta}{dY^2} = -1, \quad 0 \leqslant Y \leqslant \sigma \tag{56}$$

B.C. 2 $$U_\eta = U, \quad \frac{\partial U_\eta}{\partial Y} = \frac{\partial U}{\partial Y}, \quad Y = 0 \tag{57}$$

$$\underbrace{\frac{1}{\varepsilon_\beta}\frac{\partial^2 U}{\partial Y^2}}_{\substack{\text{first}\\ \text{Brinkman}\\ \text{correction}}} + \underbrace{\frac{1}{\varepsilon_\beta}\frac{\partial \varepsilon_\beta}{\partial Y}\left[\frac{\partial}{\partial Y}\left(\frac{1}{\varepsilon_\beta}U\right)\right]}_{\text{second Brinkman correction}}$$

$$-\underbrace{\frac{K_{\beta\omega}}{K_\beta(y)}}_{\text{Darcy stress}} U = -1, \quad -\delta/\sqrt{(K_{\beta\omega})} \leqslant Y \leqslant 0 \tag{58}$$

B.C. 3 $$U = U_\omega \quad \frac{\partial U}{\partial Y} = \frac{\partial U_\omega}{\partial Y}, \quad Y = -\delta/\sqrt{(K_{\beta\omega})} \tag{59}$$

$$\frac{1}{\varepsilon_{\beta\omega}}\frac{d^2 U_\omega}{dY^2} - U_\omega = -1, \quad -\infty \leqslant Y \leqslant 0 \tag{60}$$

B.C. 4 $$U_\omega \to 1 \quad \text{at } Y \to -\infty. \tag{61}$$

The analytical solutions for the η- and ω-regions are given by

$$U_\eta = \tfrac{1}{2}\sigma^2[1-(Y/\sigma)^2] - C_1\sigma[1-(Y/\sigma)], \quad 0 \leqslant Y \leqslant \sigma \tag{62}$$

$$U_\omega = C_2 \exp(\sqrt{(\varepsilon_{\beta\omega})}\, Y) + 1, \quad -\infty \leqslant Y \leqslant 0 \tag{63}$$

and the two velocity fields are specified in terms of *assumed* values of C_1 and C_2. An iterative procedure then leads to a numerical solution of equation (58) based on matching the derivatives at $Y = 0$ and at $-\delta/\sqrt{(K_{\beta\omega})}$. This, in turn, provides a solution for the velocity field in the η-region, and one then makes use of equation (33) to compute the fractional excess flow in terms of the adjustable parameter, $\delta/\sqrt{(K_{\beta\omega})}$. The

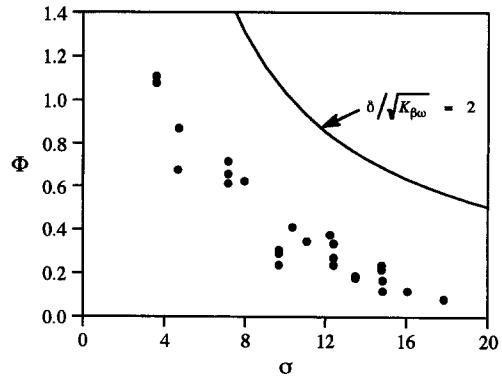

Fig. 6. Comparison between the variable porosity model and experiment for Foametal ($K_{\beta\omega} = 1.1 \times 10^{-5}$ in^2).

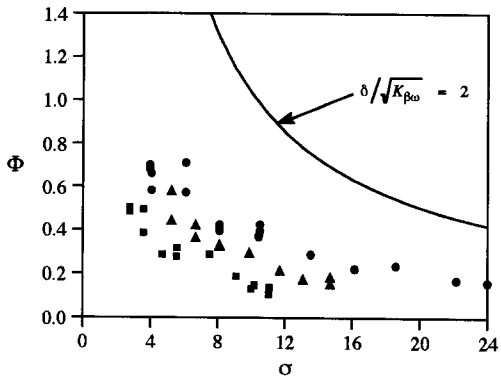

Fig. 7. Comparison between the variable porosity model and experiment for Foametal (■, $K_{\beta\omega} = 15.0 \times 10^{-6}$ in^2; ▲, $K_{\beta\omega} = 61.0 \times 10^{-6}$ in^2; ●, $K_{\beta\omega} = 127 \times 10^{-6}$ in^2).

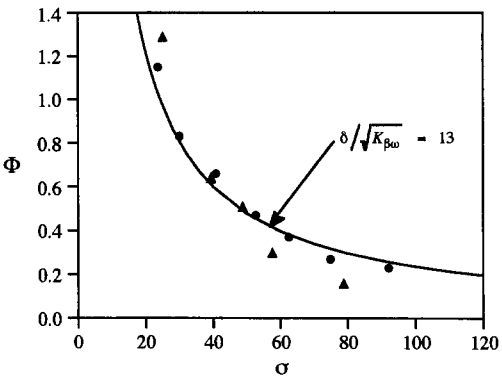

Fig. 8. Comparison between the variable porosity model and experiment for Aloxite (●, $K_{\beta\omega} = 1.0 \times 10^{-6}$ in^2; ▲, $K_{\beta\omega} = 2.48 \times 10^{-6}$ in^2).

results are displayed in Figs. 6–8. In Fig. 6 we see *poor* agreement between the model and the experimental data for the Foametal–water system for a value of $\delta/\sqrt{(K_{\beta\omega})} = 2$. A similar situation is illustrated in Fig. 7 for three Foametal–oil systems, and the use of even *smaller* values of the parameter, $\delta/\sqrt{(K_{\beta\omega})}$ leads to *larger* values of Φ. Since we expect Φ to *decrease* with *decreasing* values of $\delta/\sqrt{(K_{\beta\omega})}$ this behavior does not make physical sense and we conclude that our choice

of functions for the porosity and the permeability given by equations (53) and (54) is unacceptable for small values of $\delta/\sqrt{(K_{\beta\omega})}$. Not only do small values of $\delta/\sqrt{(K_{\beta\omega})}$ lead to physically unreasonable results, but they are also in *conflict with* the estimate given by equation (44). The failure of our variable porosity model is most likely associated with the representation for the term $\mathbf{\Phi}_\beta$ which is given exactly by equation (36) of Part I. While the limiting forms of that integral expression are correctly given by equation (39), the simplification represented by equation (54) for the local permeability would appear to be unacceptable. This is consistent with the conclusion reached by Sahraoui and Kaviany [4] on the basis of a detailed solution of the Navier–Stokes equations in the neighborhood of the boundary between a porous medium and a homogeneous fluid. A variable porosity model has also been proposed by Hsu and Cheng [6] for plane Couette flow past a porous medium; however, no comparison with experiment was carried out.

In Fig. 8 we have compared the variable porosity model with the two Aloxite–oil systems studied by Beavers and Joseph [1]. The value of $\delta/\sqrt{(K_{\beta\omega})} = 13$ for these systems provides *good* agreement with the experimental results and is *consistent* with the estimate given by equation (44). A key difference between the Foametal systems and the Aloxite systems is that the latter have permeabilities that are an order of magnitude smaller than the former.

While the results shown in Fig. 8 are certainly attractive, the overall comparison between the variable porosity model and the experimental data leaves much to be desired. The results based on the stress jump condition that were presented in Section 2 are considerably more attractive, and one must wonder why an approach that is based on a *more* accurate description of the fluid mechanics leads to a *less* attractive comparison between theory and experiment. The reason seems to be associated with the complexity of equation (58) which replaces the relatively simple stress condition given by equation (20). The three terms on the left hand side of equation (58) change significantly with position and this is illustrated in Fig. 9 where we have presented calculated values of the first Brinkman correction, $\varepsilon_\beta^{-1}\partial^2 U/\partial Y^2$, the second Brinkman correction, $\varepsilon_\beta^{-1}(\partial\varepsilon_\beta/\partial Y)\,\partial(\varepsilon_\beta^{-1}U)/\partial Y$, and the Darcy stress, $(K_{\beta\omega}/K_\beta(y))U$. There we see that the first Brinkman correction and the Darcy stress tend to cancel each other. This means that the second Brinkman correction plays a crucial role in the fluid mechanics of the boundary region even though it is smaller than the other two viscous terms. The results presented in Fig. 9 clearly indicate that the second Brinkman correction cannot, in general, be neglected as has been done in all previous studies. Sahraoui and Kaviany [4] have suggested that the permeability may be a very complex function of position in the interfacial region, and this certainly seems to be an explanation for the failure of the variable porosity model illustrated in Figs. 6 and 7. One could undoubtedly find a function $K_{\beta\omega}/K_\beta(y)$ that could be used to fit the experimental results of Beavers and Joseph; however, there is no reason to explore this possibility without more detailed laboratory experiments and numerical solutions of the Stokes' equations in the boundary region. The latter could be used to evaluate the function $\mathbf{\Phi}_\beta$ directly and this would provide extremely useful information.

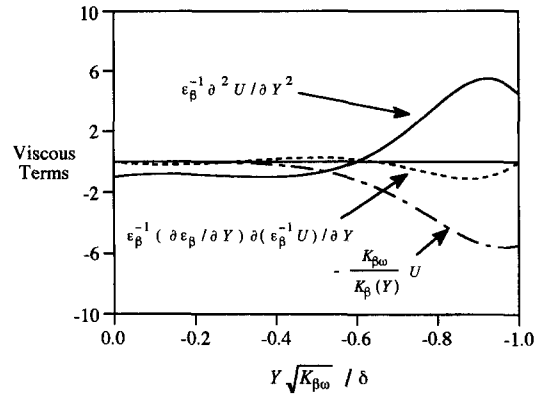

Fig. 9. Variation of Brinkman correction terms in the interfacial region.

4. CONCLUSIONS

In this paper we have developed solutions of the equations of motion for the flow of a homogeneous fluid past a porous medium, subject to a stress jump condition imposed at the boundary between these two regions. For the experimental data that are currently available, one can obtain good agreement between theory and experiment in terms of a single adjustable parameter that appears in the stress jump condition. This parameter is of order one as predicted by the theory; however, the development of a reliable empirical representation for this parameter will require further experimental studies. Attempts to develop a more rigorous description of the boundary region provide some insight into the nature of the first and second Brinkman corrections; however, detailed laboratory and numerical experiments are needed before significant improvements on the stress jump condition can be made.

Acknowledgement—The authors gratefully acknowledge the financial support provided by CONACyT (project 1231-A9203) of the Mexican government.

REFERENCES

1. G. S. Beavers and D. D. Joseph, Boundary conditions at a naturally permeable wall, *J. Fluid Mech.* **30**, 197–207 (1967).

2. R. E. Larson and J. J. L. Higdon, Microscopic flow near the surface of two-dimensional porous media—I. Axial flow, *J. Fluid Mech.* **166,** 449–472 (1987).
3. R. E. Larson and J. J. L. Higdon, Microscopic flow near the surface of two-dimensional porous media—II. Transverse flow, *J. Fluid Mech.* **178,** 119–136 (1987).
4. M. Sahraoui and M. Kaviany, Slip and no-slip velocity boundary conditions at interface of porous, plain media, *Int. J. Heat Mass Transfer* **35,** 927–943 (1992).
5. R. B. Bird, W. E. Stewart and E. N. Lightfoot, *Transport Phenomena.* John Wiley, New York (1960).
6. C. T. Hsu and P. Cheng, A singular perturbation solution for Couette flow over a semi-infinite porous bed, *J. Fluids Engng* **113,** 137–142 (1991).